

# HG-Lane: High-Fidelity Generation of Lane Scenes under Adverse Weather and Lighting Conditions without Re-annotation

Daichao Zhao<sup>1\*</sup>, Qiupu Chen<sup>2\*</sup>, Feng He<sup>3</sup>, Xin Ning<sup>4</sup>, Qiankun Li<sup>5†</sup>

<sup>1</sup>Shanghai Jiao Tong University, <sup>2</sup>School of Artificial Intelligence, Henan University,

<sup>3</sup>University of Science and Technology of China,

<sup>4</sup>AnnLab, Institute of Semiconductors, Chinese Academy of Sciences,

<sup>5</sup>Nanyang Technological University



Figure 1. **High-fidelity weather and lighting transformations generated by our HG-Lane framework.** Lane labels are preserved exactly, while the remaining scene semantics are kept consistent across Normal, Night, Dusk, Snow, Rain, and Fog conditions.

## Abstract

Lane detection is a crucial task in autonomous driving, which is conducive to ensuring the safe operation of vehicles. However, current datasets like CULane and TuSimple have relatively limited data under extreme weather conditions, such as rain, snow and fog, which makes detection models unreliable in extreme conditions, potentially leading to serious safety-critical failures on the road. In this direction, we propose **HG-Lane**, a **High-fidelity Generation** framework for **Lane** Scenes under adverse weather and lighting conditions, without the need for re-annotation. Based on our framework, we further propose a benchmark that includes adverse weather and lighting conditions, with 30,000 images. Experiment results demonstrate that our method constantly and significantly improves the performance of all the related lane detection networks. Taking the state-of-the-art CLRNNet as an example, the overall mF1 on our benchmark increases by 20.87%. The F1@50 for the overall, normal, snow, rain, fog, night, and dusk categories increases by 19.75%, 8.63%, 38.8%, 14.96%, 26.84%, 21.5%, and 12.04%, respectively. The Code and dataset are available at <https://github.com/zdc233/HG-Lane>.

## 1. Introduction

Lane detection is a crucial task in autonomous driving and Advanced Driver Assistance System (ADAS), which helps vehicles localize themselves better and drive safer.

In recent years, more and more works have demonstrated their excellent performance in the lane detection task, such as UFLD [25], RESA [44], CLRNNet [16], etc. However, most of the current state-of-the-art (SOTA) works are based on the CULane [23], TuSimple [25] and LLAMAS [2] datasets, the vast majority of whose samples are sunny and daytime scenes, lacking samples of adverse weather conditions. This deficiency causes a significant drop in the performance of detection models under adverse weather conditions, which affects the safety of autonomous driving.

Although it is possible to collect these data manually, the low frequency of adverse weather occurrences and the high cost of re-annotation make it inefficient and difficult to build in a short period of time. Besides, it should be noted that some existing works can achieve image restoration, such as WGWS-Net [45], Domain Translation Multi-weather Restoration [24], and CycleGAN [36], but they require retraining for each type of weather condition and the process of image restoration adds extra overhead, making it difficult to meet the requirements for real-time perfor-

\* Equal contribution. † Corresponding author ([qiankun.li@ntu.edu.sg](mailto:qiankun.li@ntu.edu.sg)).

mance. In addition to these methods, there are also works based on Diffusion models that achieve realistic data generation, such as WeatherDG [27] and DA-Fusion [39]. However, they still require re-annotation of data and fine-tuning of the diffusion model, which incurs additional costs.

In this paper, we present *HG-Lane*, a **High-fidelity Generative** framework that generates realistic **Lane** scenes under adverse weather and lighting conditions—such as snow, rain, fog, night, and dusk—*without requiring any re-annotation*. Specifically, we extract the normal-condition images from the CULane dataset and preprocess them with a semantic-preserving strategy that fuses Canny edges and lane annotations. These are used to guide the generative model via a dual-stage pipeline: ControlNet (Canny) handles structure preservation, while ControlNet (Instruct-Pix2Pix) refines lighting and style. By applying category-specific prompts, we successfully generate realistic lane scenes across five new adverse-condition categories.

Built upon HG-Lane, we further introduce a new benchmark consisting of 30,000 generated images across six conditions, significantly enriching the diversity of lane detection scenarios. We evaluate multiple state-of-the-art lane detection models on this benchmark and conduct comprehensive ablation studies to validate the effectiveness of each component in our framework. We also conducted ablation studies, compared multiple generative models and suppression modules, and carried out tests on real-world data. Experimental results demonstrate that the proposed method stably and significantly improves the detection accuracy of all relevant networks, exhibiting strong generalization capability and structural soundness across various settings.

The main contributions can be summarized as follows:

- We propose HG-Lane, a novel framework that generates high-fidelity lane scenes under diverse weather and lighting conditions, while **preserving lane semantics and requiring no re-annotation in a consistent manner**.
- We design a **dual-stage** generation strategy using ControlNet with Canny and InstructPix2Pix guidance, enhanced by a semantic-aware preprocessing pipeline to retain lane structure and scene consistency.
- We construct a new benchmark containing **30,000** lane images across six categories (*normal, snow, rain, fog, night, dusk*), enabling systematic evaluation of model robustness under challenging conditions.
- Extensive experiments show that our method improves lane detection accuracy across multiple models. Taking SOTA CLRNet as an example, it increases overall mF1 by 20.87%, with significant gains in all subcategories: snow (+38.8%), night (+21.5%), fog (+26.84%), etc.

## 2. Related Work

### 2.1. Generative Models

Generative models have always attracted significant attention and have seen rapid development in recent years. Early methods, such as ♣ **Variational Autoencoders (VAEs)**[17], ♣ **Generative Adversarial Networks (GANs)**[9], and ♣ **Flow-Based models** [32], have shown potential in generating images but also have certain limitations. For instance, GANs are not good at generating samples they have not observed, while VAEs and Flow-Based models are not proficient at generating high-fidelity samples. In recent years, many successes in photorealistic image generation have been achieved by Diffusion models [13] [21] [34] [22] [30]. Compared to GANs, ♣ **Diffusion models** have been proven to generate higher-fidelity samples [7], and developments such as classifier-free guidance [12] have made text-to-image generation possible.

### 2.2. Condition Control

Condition control in diffusion models has always been a research hotspot. Stable Diffusion [33], trained on the LAION-5B [35] dataset and based on CLIP [29], can achieve text-guided image generation. ♣ **ControlNet** [11] fine-tunes Stable Diffusion and uses multiple conditions to guide image generation, including text prompts and edge maps, which can better preserve the overall semantics of the image. ♣ **InstructPix2Pix** [8], on the other hand, can directly edit the original image and retain more details. Currently, combining multiple ControlNets together has shown powerful effects. For example, ComfyUI[6] provides a convenient workflow to achieve this in a highly flexible manner.

### 2.3. Lane Detection

Lane detection methods can be categorized into several approaches. Segmentation-based approaches like SCNN [23] and RESA [44], utilize pixel classification and post-clustering strategies. Row-wise classification methods such as CondLaneNet [18] enhance computational efficiency by dividing the input image into grids and predicting lanes row by row. Anchor-based methods, including UFLD [28] and ♣ **CLRNet** [16], employ various anchor strategies to improve detection of lanes. Parametric prediction methods, represented by PolyLaneNet [37] and LSTR [19], achieve end-to-end detection by modeling lane lines as curve equations. Each approach contributes uniquely to advancing lane detection capabilities within modern autonomous driving.

## 3. Method

HG-Lane is a dual-stage, control-guided diffusion framework that generates lane images with diverse weather and illumination while preserving lane geometry. Instead of fine-tuning diffusion models, HG-Lane reuses pretrained com-

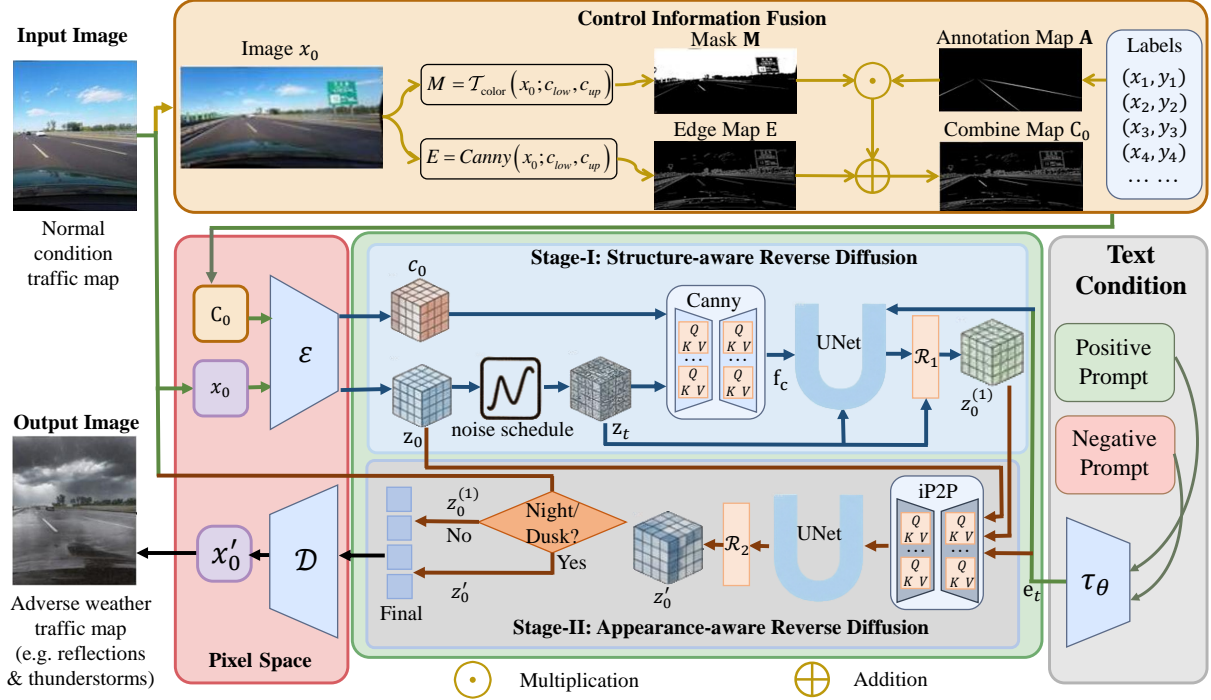


Figure 2. **Overview of the proposed HG-Lane.** The input image is first processed into a fused control map combining color-based masks, Canny edges and lane annotations. In Stage-I, a Canny-ControlNet enforces lane geometry during reverse diffusion in latent space. In Stage-II, an InstructPix2Pix ControlNet optionally refines appearance for “night” and “dusk”. Finally, the latent is decoded back to pixel space. All components are pretrained; no fine-tuning is required.

ponents and injects task-specific structure via control signals. As shown in Fig. 2, the pipeline consists of four components: (1) **Control Information Fusion** that fuses lane annotations, color masks, and Canny edges into a unified control map; (2) **Stage-I Structure-aware Reverse Diffusion** driven by a Canny-based ControlNet to enforce lane geometry; (3) **Stage-II Appearance-aware Reverse Diffusion** using an InstructPix2Pix ControlNet to refine style for selected categories (night/dusk); and (4) **Pixel-space Conversion** that decodes the latent back to the image domain.

We denote the pretrained VAE encoder and decoder as  $\mathcal{E}(\cdot)$  and  $\mathcal{D}(\cdot)$ , and the pretrained latent diffusion model (UNet backbone plus ControlNet) as  $\mathcal{U}_\phi$ , with all parameters kept frozen during our pipeline.

### 3.1. Control Information Fusion

Let the input lane image be  $\mathbf{x}_0 \in \mathbb{R}^{H \times W \times 3}$  and the corresponding lane annotation map be  $\mathbf{A} \in \{0, 1\}^{H \times W}$ . The goal of this stage is to construct a control map  $\mathbf{C}_0$  that encodes both lane geometry and local edge cues while being robust to dashed or incomplete markings.

**Geometric priors from color and edges.** We first apply a color-thresholding operator to extract lane-related regions:

$$\mathbf{M} = \mathcal{T}_{\text{color}}(\mathbf{x}_0; c_{\text{low}}, c_{\text{up}}), \quad \mathbf{M} \in \{0, 1\}^{H \times W}, \quad (1)$$

where  $c_{\text{low}}$  and  $c_{\text{up}}$  are lower and upper bounds of the color threshold and  $\mathbf{M}$  denotes the resulting mask map. In parallel, we compute the edge map using the Canny operator:

$$\mathbf{E} = \text{Canny}(\mathbf{x}_0; c_{\text{low}}, c_{\text{up}}), \quad (2)$$

where the same thresholds control edge sensitivity.

**Fusion with annotations.** To avoid over-relying on dense, continuous annotations (which may conflict with dashed lane markings), we combine them with  $\mathbf{M}$  and  $\mathbf{E}$  via:

$$\mathbf{C}_0 = (\mathbf{A} \odot \mathbf{M}) \oplus \mathbf{E}, \quad (3)$$

where  $\odot$  denotes element-wise multiplication and  $\oplus$  denotes pixel-wise logical OR (or max). Here,  $\mathbf{A} \odot \mathbf{M}$  suppresses annotation pixels outside the color-consistent region, while  $\mathbf{E}$  injects additional edge cues where Canny succeeds even if annotations are sparse or imperfect. Our ablation shows that using  $\mathbf{E}$  alone leads to missing or misaligned lanes in complex conditions, whereas  $(\mathbf{A} \odot \mathbf{M}) \oplus \mathbf{E}$  yields more reliable lane structure priors.

### 3.2. Stage-I: Structure-aware Reverse Diffusion

The first reverse diffusion stage enforces lane geometry in the latent space using the fused control map  $\mathbf{C}_0$  and a Canny-based ControlNet.

**Latent encoding and forward diffusion.** We first encode the control map and the original image into the latent space:

$$\mathbf{c}_0 = \mathcal{E}(\mathbf{C}_0), \quad \mathbf{z}_0 = \mathcal{E}(\mathbf{x}_0), \quad (4)$$

where  $\mathbf{c}_0, \mathbf{z}_0 \in \mathbb{R}^{H' \times W' \times d}$ . A standard forward diffusion process gradually corrupts  $\mathbf{z}_0$  into  $\mathbf{z}_T$ :

$$q(\mathbf{z}_t | \mathbf{z}_0) = \mathcal{N}(\sqrt{\bar{\alpha}_t} \mathbf{z}_0, (1 - \bar{\alpha}_t) \mathbf{I}), \quad t = 1, \dots, T, \quad (5)$$

where  $\{\bar{\alpha}_t\}$  is the cumulative noise schedule and  $\mathbf{z}_T$  is sampled at the end of the forward process.

**Canny-ControlNet guided denoising.** Conditioned on  $\mathbf{c}_0$  and text prompts, Stage-I reverse diffusion reconstructs a geometry-consistent latent  $\mathbf{z}_0^{(1)}$ . We use a Canny-trained ControlNet, denoted as  $\mathcal{C}_{\text{canny}}$ , together with a text encoder  $\tau_\theta$  that maps positive/negative prompts to conditional embeddings  $\mathbf{e}_t$ :

$$\mathbf{e}_t = \tau_\theta(\text{prompt}), \quad \mathbf{f}_c = \mathcal{C}_{\text{canny}}(\mathbf{c}_0, \mathbf{z}_t). \quad (6)$$

At each timestep  $t$ , the UNet backbone predicts the noise using both control features  $\mathbf{f}_c$  and prompt embedding  $\mathbf{e}_t$ :

$$\hat{\mathbf{e}}_t = \mathcal{U}_\phi(\mathbf{z}_t, t, \mathbf{e}_t, \mathbf{f}_c), \quad (7)$$

and the reverse update follows the standard DDPM/DDIM rule

$$\mathbf{z}_{t-1} = \mathcal{R}_1(\mathbf{z}_t, \hat{\mathbf{e}}_t), \quad (8)$$

where  $\mathcal{R}_1$  denotes one denoising step in Stage-I. After  $T$  steps, we obtain the Stage-I latent:

$$\mathbf{z}_0^{(1)} = \mathcal{R}_1^{(T)}(\mathbf{z}_T | \mathbf{c}_0, \text{prompt}). \quad (9)$$

This stage focuses on enforcing lane geometry and structural consistency under the Canny control.

**Cross-attention view.** Inside the Attention-UNet of  $\mathcal{U}_\phi$ , the prompt embedding  $\mathbf{e}_t \in \mathbb{R}^{n \times c}$  and latent feature  $\mathbf{z}_t \in \mathbb{R}^{(h \times w) \times c}$  interact through cross-attention:

$$\mathbf{Q} = \mathbf{z}_t \mathbf{W}^Q, \quad \mathbf{K} = \mathbf{e}_t \mathbf{W}^K, \quad \mathbf{V} = \mathbf{e}_t \mathbf{W}^V, \quad (10)$$

$$\text{Attn}(\mathbf{z}_t, \mathbf{e}_t) = \text{Softmax}\left(\frac{\mathbf{Q}\mathbf{K}^\top}{\sqrt{d}}\right) \mathbf{V}, \quad (11)$$

where  $\mathbf{W}^Q, \mathbf{W}^K, \mathbf{W}^V \in \mathbb{R}^{c \times d}$  are learned projections. This mechanism allows lane-specific prompts to modulate lane structures generated under Canny control condition.

### 3.3. Stage-II: Appearance-aware Reverse Diffusion

While Stage-I constrains lane structure, different weather or illumination categories require distinct appearance styles (e.g., night, dusk, snow, rain, fog). Stage-II introduces an InstructPix2Pix (iP2P) ControlNet to refine appearance in a targeted manner.

**Category-dependent refinement.** For categories such as “night” and “dusk”, solely using Canny control tends to preserve structure but fails to fully capture desired lighting and global tone. We therefore introduce a second reverse diffusion stage with an iP2P ControlNet, denoted  $\mathcal{C}_{\text{iP2P}}$ , which refines from  $\mathbf{z}_0^{(1)}$  toward an appearance-enhanced latent  $\mathbf{z}'_0$ :

$$\mathbf{z}'_0 = \mathcal{R}_2\left(\mathcal{C}_{\text{iP2P}}(\mathbf{z}_0^{(1)}, \mathbf{z}_0), \mathbf{z}_0^{(1)}, \text{prompt}_{\text{iP2P}}\right), \quad (12)$$

where  $\mathcal{R}_2$  denotes the second-stage denoising process and  $\text{prompt}_{\text{iP2P}}$  describes the desired style (e.g., night scene with illuminated lanes).

For categories such as “snow”, “rain” and “fog”, we empirically observe that a single Canny ControlNet already provides satisfactory visual realism. Therefore, for these categories, we skip Stage-II and simply set

$$\mathbf{z}'_0 = \mathbf{z}_0^{(1)}. \quad (13)$$

This category-dependent design is also illustrated as the gray “Optional” flowline in Fig. 2.

### 3.4. Pixel-space Conversion and Sampling Strategy

In the final step, the refined latent  $\mathbf{z}'_0$  is mapped back to pixel space using the pretrained VAE decoder:

$$\mathbf{x}'_0 = \mathcal{D}(\mathbf{z}'_0), \quad (14)$$

yielding the generated lane image under the target weather/illumination condition.

It is worth emphasizing that the entire HG-Lane framework is *training-free*: all VAEs, UNet backbones, and ControlNets are pretrained and kept frozen. In practice, we can sample multiple outputs using different random seeds,

$$\mathbf{x}_0'^{(k)} = \mathcal{D}(\mathbf{z}_0'^{(k)}), \quad k = 1, \dots, K, \quad (15)$$

evaluate them with metrics such as F1@50 and FID, and select the seed that provides the best trade-off between geometric accuracy and visual realism for deployment. This makes HG-Lane easy to plug into existing lane detection pipelines while providing controllable, high-fidelity synthetic data across a wide range of conditions.

## 4. Experiment

### 4.1. Benchmark

The normal category in our dataset is derived from the normal category in the CULane dataset, and we obtained 5k images via systematic sampling. The other five categories (snow, rain, fog, night, dusk) were generated by our framework. The training set, validation set, and test set are divided in a 7:1:2 ratio. See Table 1 for detailed information,

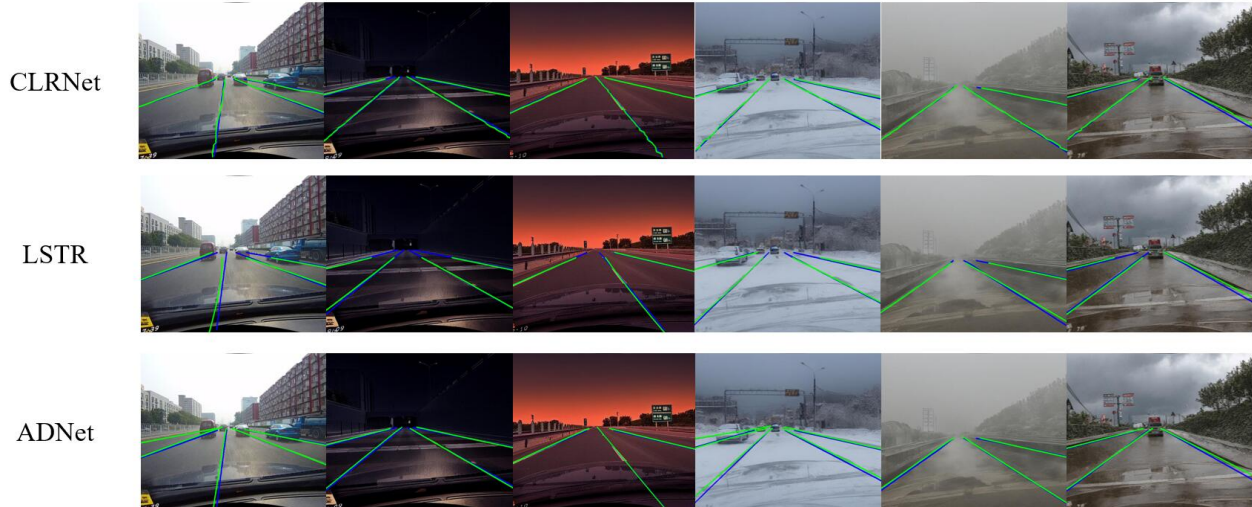


Figure 3. **Results of some baselines.** The green lines in the figure represent the predicted values, while blue lines represent ground truth.

Table 1. **The dataset generated by our framework.**

Category	Total	Train	Validate	Test
Normal	5000	3500	500	1000
Snow	5000	3500	500	1000
Rain	5000	3500	500	1000
Fog	5000	3500	500	1000
Night	5000	3500	500	1000
Dusk	5000	3500	500	1000

## 4.2. Metrics

We follow the evaluation protocol of the CULane dataset. A predicted lane point is matched to the ground truth if the Intersection over Union (IoU), computed by dilating both by 30 pixels, exceeds a threshold  $\alpha$ . True positives, false positives, and false negatives are counted to compute F1. In practice,  $\alpha$  is set to 0.5 and 0.75, reported as F1@50 and F1@75, respectively. We also compute the mean F1 (mF1) by averaging F1 scores over  $\alpha \in [0.5, 0.95]$  with a step of 0.05. For the Normal, Snow, Rain, Fog, Night, and Dusk scenarios, the primary metric is F1@50 in reported results.

## 4.3. Experimental Details

**Generate Images by Our Framework.** Our framework employs ComfUI for workflow design. The experiment is conducted on an Nvidia GeForce RTX 3090 GPU with 24 GB of memory, running the Ubuntu 24.04 operating system. The programming language used is Python 3.8.0, and the PyTorch 1.13.1 framework is employed. Reverse Diffusion 1 and 2 used the Euler sampler and the Karras scheduler, with a sampling step size of 30 and  $\text{cfg} = 6.0$ .

**Lane Detection Experiment.** Using our benchmark, we

tested SOTA and highly cited lane detection models from recent years. We employed the environment required by the official code of each model. Given the wide range of hardware requirements, we conducted the tests on multiple servers with different specifications. We uniformly set the training epochs = 12, and use the best model to test.

## 4.4. Comparison Experiment

We utilized CLRNet (ResNet-18) to test both the pre-augmented and post-augmented datasets. The test sets consist of 6 categories (normal, snow, rain, fog, night, dusk), each with 1,000 images. To eliminate the interference of dataset size on the results, before augmentation, we used 3,500 training + 500 validation normal images as one dataset, and another dataset with  $6 \times (3,500 \text{ training} + 500 \text{ validation})$  normal images. After augmentation, we used datasets with 6 categories, each containing 3,500 training + 500 validation images. This ensures a consistent number of normal images used for training and validation, as well as a consistent total number of images.

The experimental results are shown in Table 2. We observe that F1@50 for the normal, snow, rain, fog, night, and dusk categories increased by 8.63%, 38.8%, 14.96%, 26.84%, 21.5%, and 12.04%, with an overall improvement of 19.75%. This validates that the data we generated addresses the robustness issue of the model under adverse weather and lighting conditions.

## 4.5. Performance on various baselines

As shown in Table 3, we conducted tests on the state-of-the-art (SOTA) and highly cited lane detection baselines in recent years, such as FENet [41], CLRKNet [26], CLRRNet [14], ADNet [43], CLRNet [16], GANet [40], CondLaneNet [18], LaneATT [38], LaneAF [1], RESA [44],

Table 2. Performance on CLRNet (ResNet-18). For Normal, Snow, Rain, Fog, Night, and Dusk, the metric used is F1@50.

Method	Normal	Snow	Rain	Fog	Night	Dusk	F1@50	F1@75	mF1
w/o aug (4k)	83.01	46.08	70.34	58.54	70.09	79.95	68.74	46.39	42.16
w/o aug (4k*6)	87.28	51.79	71.48	58.31	62.67	75.62	68.89	50.87	45.42
<b>w/ aug (4k*6)</b>	<b>91.64</b>	<b>84.88</b>	<b>85.30</b>	<b>85.38</b>	<b>91.59</b>	<b>91.99</b>	<b>88.49</b>	<b>72.79</b>	<b>63.03</b>

Table 3. Performance comparison on CULane benchmarks. For Normal, Snow, Rain, Fog, Night, and Dusk, the metric is F1@50 to provide a clearer comparison across different environmental conditions. Best results are in **bold**, second best are underlined.

Method	Normal	Snow	Rain	Fog	Night	Dusk	F1@50	F1@75	mF1
<b>Classical / Light Backbones</b>									
SCNN (ResNet-34)[23]	75.91	68.96	67.56	62.54	70.51	70.46	72.97	31.34	20.08
SAD (ENet)[15]	76.75	64.71	68.85	61.73	73.39	76.68	70.02	30.91	19.36
LSTR (ResNet-34)[19]	84.06	74.67	76.61	74.40	83.71	84.38	65.07	59.75	16.48
<b>UFLD / RESA Family</b>									
UFLD (ResNet-18)[28]	69.59	59.29	60.77	56.52	59.69	63.97	61.65	17.56	13.42
UFLD (ResNet-34)[28]	74.42	62.52	66.28	64.72	72.77	74.01	69.14	18.99	14.61
RESA (ResNet-18)[44]	78.44	69.28	70.17	69.41	77.34	78.47	73.86	28.29	19.85
RESA (ResNet-34)[44]	77.31	68.90	69.20	69.12	77.42	77.71	73.38	27.58	19.36
<b>LaneATT / LaneAF / CondLaneNet Family (Modern CNN Baselines)</b>									
LaneATT (ResNet-18)[38]	81.78	72.55	73.17	71.48	80.53	80.75	76.75	44.71	34.02
LaneATT (ResNet-34)[38]	81.92	72.77	73.34	71.49	80.63	80.88	76.99	45.01	34.18
LaneAF (ERFNet)[1]	<u>89.63</u>	84.98	84.56	84.78	89.12	89.63	86.66	67.01	58.78
LaneAF (DLA-34)[1]	90.63	85.15	84.94	85.19	90.02	90.21	87.70	67.72	59.98
CondLaneNet (ResNet-18)[18]	90.58	83.52	84.15	84.59	90.04	89.89	88.44	68.76	59.05
CondLaneNet (ResNet-34)[18]	91.05	84.35	85.31	84.98	90.56	90.14	88.53	69.56	59.87
<b>CLR / CLRKD / GANet Family (State-of-the-art CNN Lanes)</b>									
GANet (ResNet-18)[40]	93.22	88.01	88.55	88.34	92.59	94.36	90.88	75.31	66.18
GANet (ResNet-34)[40]	<u>93.96</u>	<u>88.95</u>	<u>88.89</u>	<u>88.78</u>	<u>93.30</u>	93.54	91.25	75.55	66.89
CLRNet (ResNet-18)[16]	91.64	84.88	85.30	85.38	91.59	91.99	88.49	72.79	63.03
CLRNet (ResNet-34)[16]	91.25	80.96	85.24	83.15	91.15	91.84	87.38	70.76	60.89
ADNet (ResNet-18)[43]	81.03	70.76	74.29	72.11	81.12	82.09	76.98	51.59	42.33
ADNet (ResNet-34)[43]	81.89	71.20	75.89	73.33	81.89	82.65	77.37	52.02	42.84
CLRerNet[14]	92.34	82.54	85.47	85.33	91.54	91.88	90.68	76.27	65.31
CLRKDNet (ResNet-18)[26]	92.15	85.33	85.46	85.52	92.02	92.69	88.53	73.11	64.01
CLRKDNet (DLA34)[26]	92.52	85.62	85.74	85.33	91.99	93.21	88.92	73.49	64.75
<b>FENet[41]</b>	<b>95.78</b>	<b>89.47</b>	<b>90.28</b>	<b>95.05</b>	<b>95.68</b>	<b>90.43</b>	<b>92.76</b>	<b>82.17</b>	<b>69.66</b>

LSTR [19], UFLD [28], SAD [15], SCNN [23].

All our training configurations are based on the open-source code of the respective baselines, with only the same epoch set to 12 and without using any pre-trained weights. The results demonstrate that our dataset exhibits good compatibility across all the baselines under diverse evaluation settings.

As shown in Figure 3, we present partial results of the baseline on six categories. The green lines represent the predicted values, while the blue lines represent the ground truth. It can be observed that the two lines fit well with each other. We specifically list ADNet, and it can be found that it also predicts the leftmost lane line, even though this lane line is not labeled in the CULane dataset.

## 4.6. Ablation Study

In Table 4, we conducted ablation studies on the pipeline and Preprocess design of our framework. The results of experiments #1 and #5 show that fusing lane line labels as a mask into the Canny image is beneficial, with an increase of 1.68% in F1@50. The results of experiments #1, #2, #3, and #4 indicate that using Canny or InstructP2P alone for control, or swapping the order of Canny and InstructP2P in our framework, may lead to suboptimal results. The images listed in Figure 4 intuitively demonstrate this point, showing that the labels and semantic information are invisible.

This phenomenon can be likened to the process of painting: the Canny image acts as a geometric sketch, delineating the boundaries for the model and indicating “*where the edges lie*,” yet it falls short of pixel-level precision and in-



Figure 4. **Ablation Study.** Experiment #1, #2, #3, and #4 demonstrate the generation results of using Canny or InstructPix2Pix individually, as well as the effects of their combined order.

Table 4. **Ablation study.** The symbol  $\checkmark$  indicates whether it is used, while "before" and "after" denote the sequence of usage.

#	Mask	Canny	iP2P	F1@50	F1@75	mF1
1	$\checkmark$	$\checkmark$ before	$\checkmark$ after	<b>88.49</b>	<b>72.79</b>	<b>63.03</b>
2	$\checkmark$	$\checkmark$ after	$\checkmark$ before	62.56	41.01	39.44
3	$\checkmark$		$\checkmark$	59.75	40.33	39.33
4	$\checkmark$	$\checkmark$		64.01	43.78	40.12
5		$\checkmark$ before	$\checkmark$ after	86.81	70.12	61.35

evitably introduces noise. InstructP2P supplies the color, informing the model "what the hues should be," and is capable of pixel-accurate control.

When generating night or dusk scenes, sketching the skeleton first and then applying color ensures that the sky tones remain within plausible bounds without importing extraneous noise or spurious features. Reversing the order—coloring before outlining—allows the pigments to overflow the skeletal confines, and the attendant noise seeds unwanted artifacts across the canvas. For adverse-weather conditions such as snow, rain, or fog, we actually desire the emergence of pixel-level stochasticity (snowflakes, rain streaks, misty veil), so the tight pixel-level grip of InstructP2P is deliberately relaxed.

The rationale for fusing lane-line annotations into the control signal is to preserve label invariance: the lane positions are pre-etched into the geometric skeleton, guaranteeing their immutability throughout the generative process. Positive and negative prompts constrain the model toward the desired generative behavior while discouraging the production of irrelevant.

It is worth highlighting that, despite the degraded quality of some generated images, the F1@50, F1@75, and mF1 scores remain non-zero. This is attributable to the presence of normal-condition samples in the training data, which provide the model with stable prior knowledge.

## 4.7. Quality Analysis of Generation

We also tested the quality of the images generated by our proposed framework and compared it with Stable Diffusion [33], PITI [42], CycleGAN[36] and Flux.1 with the results shown in Table 5.

Table 5. **Generative Quality.** The symbol  $\uparrow$  indicates that the higher the value of item, the better. The symbol  $\downarrow$  is opposite.

Method	F1@50 $\uparrow$	FID $\downarrow$	CLIP-T score $\uparrow$	Human score $\uparrow$
Stable Diffusion	69.02	236.7	0.20	2.35 $\pm$ 0.75
PITI	390.5	58.50	0.16	1.1 $\pm$ 0.31
CycleGAN	81.49	99.8	0.22	3.75 $\pm$ 0.55
Flux.1	70.04	120.3	0.21	2.5 $\pm$ 0.61
<b>HG-Lane(Ours)</b>	<b>80.1</b>	<b>0.23</b>	<b>88.49</b>	<b>4.15 <math>\pm</math> 0.59</b>

We conducted a human survey among 20 strangers, inviting them to rate the realism of the generated images on a scale from 1 to 5, where 1 indicates extremely unrealistic and 5 indicates extremely realistic. The resulting Human score is displayed. We used the same generation prompts to test the CLIP-T score. We also tested the F1@50 using CLNet (ResNet-18) to verify whether the lane line detection performance has changed. The results show that our proposed framework outperforms the others.

Figure 5 also demonstrates this point, showing that while Stable Diffusion performs well in preserving lane line labels, it falls short in terms of realism and semantic information retention. On the other hand, PITI leans towards an artistic style, which is not suitable for our task.

## 4.8. Performance on Real World

To evaluate our framework’s generalization ability in the real world, we collected real-world samples, annotated and processed them according to the CULane requirements, and obtained 200 images each for snow, rain, fog, night, and dusk. We then tested them with CLNet (ResNet-18), and

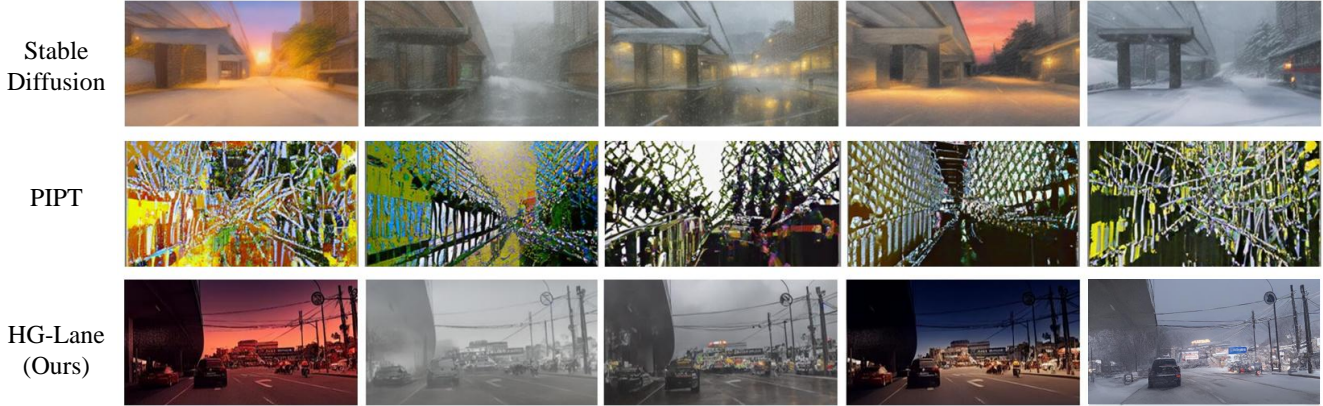


Figure 5. **Quality Analysis of Generation.** Comparison of images generated by different frameworks. The figure illustrates the generation results of different frameworks across five categories (dusk, fog, rain, night, and snow).

Table 6. **Performance on CLRNNet (ResNet-18) in Real world.** For Normal, Snow, Rain, Fog, Night, and Dusk, the metric used is F1@50.

Train on	Snow	Rain	Fog	Night	Dusk	F1@50	F1@75	mF1
CULane	35.41	74.78	50.00	22.47	20.77	53.03	21.62	25.65
<b>HG-Lane(Ours)</b>	<b>55.65</b>	<b>77.58</b>	<b>65.57</b>	<b>60.02</b>	<b>69.31</b>	<b>68.54</b>	<b>27.48</b>	<b>32.75</b>

the results are shown in Table 6. Compared with the model trained on the same amount of original CULane data, our model achieves substantial improvements on all five categories, with the overall F1@50 increasing by 15.51 %.

#### 4.9. Compare with Suppression Module

To compare the difference between our framework and directly adding weather-suppression modules, we tested our self-collected real-world rain, snow, and fog samples on their respective weather categories using F1@50.

We also measured the overhead time of these suppression modules on an RTX-3090, with results shown in Table 7. The modules include EfficientDeRain[10] and NeRD-Rain[5] for deraining, DeSnowNet[20] and HDCW-Net[4] for desnowing, and NLD[3] and GFN[31] for defogging. Our framework demonstrates superior performance across all cases.

Table 7. **Performance on CLRNNet (ResNet-18).**

Category	Method	F1@50	Time(ms/img)
DeRain	EfficientDeRain	74.82	4.8
	NeRD-Rain	74.86	9.2
	<b>HG-Lane(Ours)</b>	<b>77.58</b>	<b>0</b>
DeSnow	DeSnowNet	35.21	10.2
	HDCW-Net	37.21	6.3
	<b>HG-Lane(Ours)</b>	<b>55.65</b>	<b>0</b>
DeFog	NLD	51.58	5.1
	GFN	53.20	7.4
	<b>HG-Lane(Ours)</b>	<b>65.57</b>	<b>0</b>

## 5. Conclusion

In this paper, we present a high-fidelity lane scene generative framework (HG-Lane). It can synthesize realistic adverse-weather and lighting scenes while preserving lane semantics, without the need for re-annotation and fine-tuning. Based on the images generated by our framework, we construct a new benchmark that includes 6 categories (normal, snow, rain, fog, night, dusk), consisting of 30,000 images. The experimental results show that our method effectively improves the performance of detection models. Using the SOTA model CLRNNet, the overall mF1 on our benchmark increased by 20.87%. The F1@50 for the overall, normal, snow, rain, fog, night, and dusk categories increased by 19.75%, 8.63%, 38.8%, 14.96%, 26.84%, 21.5%, and 12.04%.

We also provide the F1@50 scores on various baselines, which show excellent performance. Additionally, ablation studies confirm the soundness of our design; comparisons with multiple generative models demonstrate its superiority in preserving label semantics and photorealism; tests on real-world datasets verify its generalization capability; and benchmarking against the suppression module highlights its advantages in tackling the same task.

**Future Work:** HG-Lane is designed to preserve lane annotations during generation, which may inevitably introduce some location bias. In the future, we plan to explore strategies to mitigate effect while maintaining label consistency.

## Acknowledgments

This work was supported by the Key Research and Development Promotion Projects in Henan Province (Grant No. 262102210114).

## References

- [1] Hala Abualsaud, Sean Liu, David Lu, Kenny Situ, Akshay Rangesh, and Mohan M. Trivedi. Laneaf: Robust multi-lane detection with affinity fields. *IEEE Robotics Autom. Lett.*, 6(4):7477–7484, 2021. 5, 6
- [2] Karsten Behrendt and Ryan Soussan. Unsupervised labeled lane markers using maps. In *Proceedings of the IEEE International Conference on Computer Vision*, 2019. 1
- [3] Dana Berman, Tali Treibitz, and Shai Avidan. Non-local image dehazing. In *2016 IEEE Conference on Computer Vision and Pattern Recognition, CVPR 2016, Las Vegas, NV, USA, June 27-30, 2016*, pages 1674–1682. IEEE Computer Society, 2016. 8
- [4] Wei-Ting Chen, Hao-Yu Fang, Cheng-Lin Hsieh, Cheng-Che Tsai, I-Hsiang Chen, Jian-Jiun Ding, and Sy-Yen Kuo. ALL snow removed: Single image desnowing algorithm using hierarchical dual-tree complex wavelet representation and contradict channel loss. In *2021 IEEE/CVF International Conference on Computer Vision, ICCV 2021, Montreal, QC, Canada, October 10-17, 2021*, pages 4176–4185. IEEE, 2021. 8
- [5] Xiang Chen, Jinshan Pan, and Jiangxin Dong. Bidirectional multi-scale implicit neural representations for image deraining. In *IEEE/CVF Conference on Computer Vision and Pattern Recognition, CVPR 2024, Seattle, WA, USA, June 16-22, 2024*, pages 25627–25636. IEEE, 2024. 8
- [6] ComfyAnonymous. Comfyui: The most powerful and modular stable diffusion gui with a graph/nodes interface. <https://github.com/Comfy-Org/ComfyUI>, 2023. 2
- [7] Prafulla Dhariwal and Alex Nichol. Diffusion models beat gans on image synthesis. *arXiv preprint arXiv:2105.05233*, 2021. 2
- [8] Wei Dong, Shijie Xue, Xintong Duan, and Shuai Han. Prompt tuning inversion for text-driven image editing using diffusion models. In *Proceedings of the IEEE/CVF International Conference on Computer Vision (ICCV)*, 2023. 2
- [9] Ian Goodfellow, Jean Pouget-Abadie, Mehdi Mirza, Bing Xu, David Warde-Farley, Sherjil Ozair, Aaron Courville, and Yoshua Bengio. Generative adversarial nets. In *Advances in neural information processing systems*, 2014. 2
- [10] Qing Guo, Jingyang Sun, Felix Juefei-Xu, Lei Ma, Xiaofei Xie, Wei Feng, Yang Liu, and Jianjun Zhao. Efficientderain: Learning pixel-wise dilation filtering for high-efficiency single-image deraining. In *Thirty-Fifth AAAI Conference on Artificial Intelligence, AAAI 2021, Thirty-Third Conference on Innovative Applications of Artificial Intelligence, IAAI 2021, The Eleventh Symposium on Educational Advances in Artificial Intelligence, EAAI 2021, Virtual Event, February 2-9, 2021*, pages 1487–1495. AAAI Press, 2021. 8
- [11] Alon Hertz, Roy Molady, Josh Tenenbaum, Kfir Aberman, Yael Pritch, and Daniel Cohen-Or. Plug-and-play diffusion features for text-driven image-to-image translation. In *Proceedings of the IEEE/CVF Conference on Computer Vision and Pattern Recognition (CVPR)*, 2023. 2
- [12] Jonathan Ho and Tim Salimans. Classifier-free diffusion guidance. *arXiv preprint arXiv:2207.12598*, 2022. 2
- [13] Jonathan Ho, Ajay Jain, and Pieter Abbeel. Denoising diffusion probabilistic models. In *Advances in Neural Information Processing Systems*, pages 6840–6851, 2020. 2
- [14] Hiroto Honda and Yusuke Uchida. Clrnet: Improving confidence of lane detection with laneiou. In *IEEE/CVF Winter Conference on Applications of Computer Vision, WACV 2024, Waikoloa, HI, USA, January 3-8, 2024*, pages 1165–1174. IEEE, 2024. 5, 6
- [15] Yuenan Hou, Zheng Ma, Chunxiao Liu, and Chen Change Loy. Learning lightweight lane detection cnns by self attention distillation. In *2019 IEEE/CVF International Conference on Computer Vision, ICCV 2019, Seoul, Korea (South), October 27 - November 2, 2019*, pages 1013–1021. IEEE, 2019. 6
- [16] Yuhang Hu, Zihao Zhang, Yaxing Wang, Sheng Liu, Jingbo Wang, Fei Wang, Xue Liu, and Shengjin Wang. Clrnet: Cross layer refinement network for lane detection. In *IEEE/CVF Conference on Computer Vision and Pattern Recognition (CVPR)*, pages 10229–10238, 2022. 1, 2, 5, 6
- [17] Diederik P. Kingma and Max Welling. Auto-encoding variational bayes. In *2nd International Conference on Learning Representations, ICLR 2014, Banff, AB, Canada, April 14-16, 2014, Conference Track Proceedings*, 2014. 2
- [18] Lizhe Liu, Xiaohao Chen, Siyu Zhu, and Ping Tan. Condlanenet: a top-to-down lane detection framework based on conditional convolution. In *2021 IEEE/CVF International Conference on Computer Vision, ICCV 2021, Montreal, QC, Canada, October 10-17, 2021*, pages 3753–3762. IEEE, 2021. 2, 5, 6
- [19] R. Liu, Z. Yuan, T. Liu, and Z. Xiong. End-to-end lane shape prediction with transformers. In *Proceedings of the IEEE Winter Conference on Applications of Computer Vision (WACV)*, pages 3693–3701, 2021. 2, 6
- [20] Yun-Fu Liu, Da-Wei Jaw, Shih-Chia Huang, and Jenq-Neng Hwang. Desnownet: Context-aware deep network for snow removal. *IEEE Trans. Image Process.*, 27(6):3064–3073, 2018. 8
- [21] Alexander Quinn Nichol and Prafulla Dhariwal. Improved denoising diffusion probabilistic models. In *Proceedings of the 38th International Conference on Machine Learning, ICML 2021, 18-24 July 2021, Virtual Event*, pages 8162–8171. PMLR, 2021. 2
- [22] Alexander Quinn Nichol, Prafulla Dhariwal, Aditya Ramesh, Pranav Shyam, Pamela Mishkin, Bob McGrew, Ilya Sutskever, and Mark Chen. GLIDE: towards photorealistic image generation and editing with text-guided diffusion models. In *International Conference on Machine Learning, ICML 2022, 17-23 July 2022, Baltimore, Maryland, USA*, pages 16784–16804. PMLR, 2022. 2
- [23] Xingang Pan, Jianping Shi, Ping Luo, Xiaogang Wang, and Xiaoou Tang. Spatial as deep: Spatial cnn for traffic scene

- understanding. In *AAAI Conference on Artificial Intelligence (AAAI)*, 2018. 1, 2, 6
- [24] Prashant W. Patil, Sunil Gupta, Santu Rana, Svetha Venkatesh, and Subrahmanyam Murala. Multi-weather image restoration via domain translation. In *Proceedings of the IEEE/CVF International Conference on Computer Vision (ICCV)*, pages 21696–21705, 2023. 1
- [25] Fabio Pizzati, Marco Allodi, Alejandro Barrera, and Fernando García. Lane detection and classification using cascaded cnns, 2019. 1
- [26] Weiqing Qi et al. Clrkdnet: Speeding up lane detection with knowledge distillation. In *IEEE Intelligent Transportation Systems Conference (ITSC)*, 2024. 5, 6
- [27] Chenghao Qian, Yuhu Guo, Yuhong Mo, and Wenjing Li. Weatherdgc: Llm-assisted procedural weather generation for domain-generalized semantic segmentation. *IEEE Robotics Autom. Lett.*, 10(6):5919–5926, 2025. 2
- [28] Z. Qin, P. Zhang, and X. Li. Ultra fast structure-aware deep lane detection. In *Computer Vision—ECCV 2020: 16th European Conference*, pages 276–291, 2020. 2, 6
- [29] Alec Radford, Jong Wook Kim, Chris Hallacy, Aditya Ramesh, Gabriel Goh, Sandhini Agarwal, Girish Sastry, Amanda Askell, Pamela Mishkin, Jack Chen, et al. Learning transferable visual models from natural language supervision. In *Proceedings of the 38th International Conference on Machine Learning*, pages 8748–8763, 2021. 2
- [30] Aditya Ramesh, Prafulla Dhariwal, Alex Nichol, Casey Chu, and Mark Chen. Hierarchical text-conditional image generation with clip latents. *arXiv preprint arXiv:2204.06125*, 2022. 2
- [31] Wenqi Ren, Lin Ma, Jiawei Zhang, Jinshan Pan, Xiaochun Cao, Wei Liu, and Ming-Hsuan Yang. Gated fusion network for single image dehazing. In *2018 IEEE Conference on Computer Vision and Pattern Recognition, CVPR 2018, Salt Lake City, UT, USA, June 18-22, 2018*, pages 3253–3261. Computer Vision Foundation / IEEE Computer Society, 2018. 8
- [32] Danilo Jimenez Rezende and Shakir Mohamed. Variational inference with normalizing flows. In *International Conference on Machine Learning*, pages 1530–1538, 2015. 2
- [33] Robin Rombach, Andreas Blattmann, Dominik Lorenz, Patrick Esser, and Björn Ommer. High-resolution image synthesis with latent diffusion models. In *IEEE/CVF Conference on Computer Vision and Pattern Recognition, CVPR 2022, New Orleans, LA, USA, June 18-24, 2022*, pages 10674–10685. IEEE, 2022. 2, 7
- [34] Chitwan Saharia, William Chan, Saurabh Saxena, Lala Li, Jay Whang, Emily L Denton, Kamyar Ghasemipour, Raphael Gontijo Lopez, Burcu Karagol Ayan, Tim Salimans, et al. Photorealistic text-to-image diffusion models with deep language understanding. In *Advances in Neural Information Processing Systems*, pages 36479–36494, 2022. 2
- [35] Christoph Schuhmann, Romain Beaumont, Richard Vencu, Cade W Gordon, Ross Wightman, Mehdi Cherti, Theo Coombes, Aarush Kutta, Clayton Mullis, Mitchell Wortsman, et al. Laion-5b: An open large-scale dataset for training next generation image-text models. In *NeurIPS Datasets and Benchmarks Track*, 2022. 2
- [36] Xiaotao Shao, Caike Wei, Yan Shen, and Zhongli Wang. Feature enhancement based on cyclegan for nighttime vehicle detection. *IEEE Access*, 9:849–859, 2021. 1, 7
- [37] L. Tabelini, R. Berriel, T.M. Paixao, C. Badue, A.F. De Souza, and T. Oliveira-Santos. Polylanenet: Lane estimation via deep polynomial regression. In *Proceedings of the IEEE/CVF Conference on Computer Vision and Pattern Recognition (CVPR)*, pages 1234–1243, 2021. 2
- [38] Lucas Tabelini Torres, Rodrigo Ferreira Berriel, Thiago M. Paixão, Claudine Badue, Alberto F. De Souza, and Thiago Oliveira-Santos. Keep your eyes on the lane: Real-time attention-guided lane detection. In *IEEE Conference on Computer Vision and Pattern Recognition, CVPR 2021, virtual, June 19-25, 2021*, pages 294–302. Computer Vision Foundation / IEEE, 2021. 5, 6
- [39] Brandon Trabucco, Kyle Doherty, Max Gurinas, and Ruslan Salakhutdinov. Effective data augmentation with diffusion models. In *The Twelfth International Conference on Learning Representations, ICLR 2024, Vienna, Austria, May 7-11, 2024*. OpenReview.net, 2024. 2
- [40] Jinsheng Wang, Yinchao Ma, Shaofei Huang, Tianrui Hui, Fei Wang, Chen Qian, and Tianzhu Zhang. A keypoint-based global association network for lane detection. In *IEEE/CVF Conference on Computer Vision and Pattern Recognition, CVPR 2022, New Orleans, LA, USA, June 18-24, 2022*, pages 1382–1391. IEEE, 2022. 5, 6
- [41] Liman Wang and Hanyang Zhong. Fenet: Focusing enhanced network for lane detection. In *IEEE International Conference on Multimedia and Expo, ICME 2024, Niagara Falls, ON, Canada, July 15-19, 2024*, pages 1–6. IEEE, 2024. 5, 6
- [42] Tengfei Wang, Ting Zhang, Bo Zhang, Hao Ouyang, Dong Chen, Qifeng Chen, and Fang Wen. Pretraining is all you need for image-to-image translation. *arXiv:2205.12952*, 2022. 7
- [43] Lingyu Xiao, Xiang Li, Sen Yang, and Wankou Yang. Adnet: Lane shape prediction via anchor decomposition. In *Proceedings of the IEEE/CVF International Conference on Computer Vision (ICCV)*, pages 6404–6413, 2023. 5, 6
- [44] Tu Zheng, Hao Fang, Yi Zhang, Wenjian Tang, Zheng Yang, Haifeng Liu, and Deng Cai. Resa: Recurrent feature-shift aggregator for lane detection. In *Proceedings of the AAAI Conference on Artificial Intelligence*, pages 3547–3554, 2021. 1, 2, 5, 6
- [45] Yurui Zhu, Tianyu Wang, Xueyang Fu, Xuanyu Yang, Xin Guo, Jifeng Dai, Yu Qiao, and Xiaowei Hu. Learning weather-general and weather-specific features for image restoration under multiple adverse weather conditions. In *Proceedings of the IEEE/CVF Conference on Computer Vision and Pattern Recognition (CVPR)*, pages 21747–21758, 2023. 1

# HG-Lane: High-Fidelity Generation of Lane Scenes under Adverse Weather and Lighting Conditions without Re-annotation

## Supplementary Material

### A. Visualization in Real-World

In Figure 6, a comparison is presented between the samples generated by our framework and real-world samples. We can see that the realism of images generated by HG-Lane is very close to that of real-world images.



Figure 6. Comparison with Real-World Samples.

### B. Visualization in Suppression Module

In Figure 7, the samples produced by our framework are compared with those from the suppression module. We can see that the addition of the suppression module has some effect on removing weather features such as rain streaks, haze, and snowflakes, but it does not fundamentally alter the

weather domain. As a result, the lane detection model still exhibits poor generalization performance. Moreover, the suppression module itself incurs additional computational overhead, significantly impacting real-time performance.

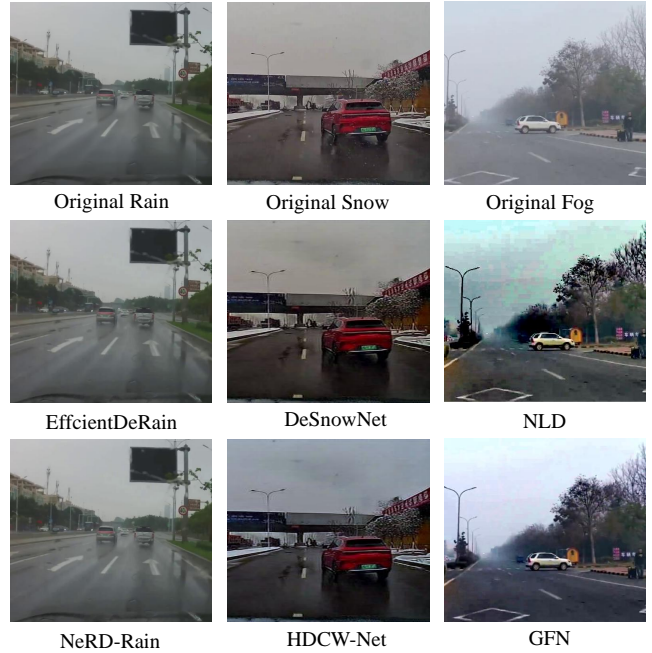


Figure 7. Comparison with Suppression Module.

### C. Visualization in Other Dataset

In Figure 8, we show our framework generalizes well to other mainstream lane detection datasets, such as Tusimple, Curvelanes, and Openlane, achieving favorable results.



Figure 8. Examples of other datasets.